Journal of Alloys and Compounds 509 (2011) 9816–9820

Contents lists available at ScienceDirect

Journal of Alloys and Compounds

journal homepage: www.elsevier.com/locate/jallcom

Low temperature sintering of ZrC–SiC composite

Liyou Zhao, Dechang Jia*, Xiaoming Duan, Zhihua Yang, Yu Zhou

Institute for Advanced Ceramics, Harbin Institute of Technology, Harbin 150001, China

ARTICLE INFO

Article history:
Received 28 April 2011
Received in revised form 25 July 2011
Accepted 8 August 2011
Available online 16 August 2011

Keywords:
Ceramics
Sintering
Microstructure

ABSTRACT

High-energy ball milling and spark plasma sintering were adopted to prepare ZrC–SiC composite. Zirconium carbide, silicon, and graphite powders were used as raw materials. ZrC–30 vol.%SiC was sintered to a relative density of >96.1% at 1800 °C. The composite showed a fine microstructure. The fracture strength reached up to 523.4 MPa, Vickers' hardness 18.8 GPa, fracture toughness 4.0 MPa $m^{1/2}$, and elastic modulus 390.5 GPa.

1. Introduction

Zirconium carbide (ZrC) is an important structural ceramic. Besides high melting temperature, ZrC has a unique combination of high fracture strength, high electrical and thermal conductivities, and resistance to erosion/corrosion [1]. ZrC is suitable for many applications such as field emitters, coating of nuclear particle fuels and ultrahigh-temperature environments [2–5]. Despite possessing useful properties, the use of monolithic ZrC is strongly limited by its poor sinterability and oxidation resistance. SiC is one of the most successful additives to improve sinterability, oxidation resistance and mechanical properties of ceramic matrix. Ma et al. [6] prepared ZrC–20 vol.%SiC composite by conventional hot pressing (HP) at 1900 °C with applied pressure of 30 MPa, and the relative density reached up to 95%. This relative density is higher than that (92.2%) of monolithic ZrC sintered with similar condition [3]. ZrC–SiC has much better oxidation resistance than monolithic ZrC [7]. Therefore, ZrC–SiC is a promising ceramic composite. However, the reports on ZrC–SiC composite are scant by far [8–11]; in particular, little work has been carried out on the sintering of ZrC–SiC composite.

Spark plasma sintering (SPS) is a good method to sinter materials with poor sinterability. High-energy plasma can bring about some phenomena that can enhance densification such as particle surface activation, local melting, and evaporation on the surface of the powder particles [12,13]. High-energy ball milling (HEBM) is usually adopted to enhance the sinterability of raw powders. Ball milling can produce much finer particles with larger surface area and also activate them mechanically via the introduction of high concentration defects, which is beneficial to increasing the diffusion coefficient and speeding up the densification kinetics [14,15]. Therefore, combination of HEBM and SPS is believed to sinter high density ZrC–SiC ceramic at relatively low temperature. This is indeed the objective of the present study.

2. Experimental

The starting powders were commercial ZrC, graphite and silicon (Si). SiC was introduced into ZrC matrix in the form of graphite and Si with molar ratio of 1:1. The volume fraction of SiC was chosen as 30 vol.% in this study. The powder mixture with above stoichiometry was high-energy ball milled under high-purity argon gas using Si_3N_4 balls and Si_3N_4 pot. The ball-to-powder weight ratio was 17:1, milling speed was 400 rpm, and milling time was 30 h. The long hours milling is to make distribution of particle size more uniform. The milled powders were put into a cylindrical carbon die with an inner diameter of 20 mm and then sintered using an SPS apparatus at 1800 °C or 1900 °C for 5 min under uniaxial pressure of 45 MPa in a vacuum (less than 5.0 Pa). The heating rate was 100 °C/min and fast cooling was achieved by switching the power off. The densities of consolidated specimens were obtained using the Archimedes method. The theoretical density of the specimen was calculated according to the rule of mixtures. Flexure strength was tested in three-point bending on 2 mm × 3 mm × 19 mm bars, using a 16 mm span and a crosshead speed of 0.5 mm/min. The reported flexure strength was the average of three measurements. Vickers' hardness was measured on polished sections by Vickers' indentation with 2 kg load holding for 10 s. Fracture toughness (K_{IC}) was evaluated by the direct crack measurement (DCM) method, using the equation of Anstis et al. [16]. The milled powders were characterized by X-ray diffractometer (XRD), transmission electron microscopy (TEM), scanning electron microscopy (SEM), Fourier transform infrared spectrometry (FTIR), Raman scattering spectroscopy, laser diffraction particle size analyzer, and nitrogen adsorption according to the method of Brunauer, Emmett, and Teller. Microstructure observation of the ceramic sample was conducted using SEM and TEM.

* Corresponding author. Tel.: +86 451 86418792; fax: +86 451 86414291.
E-mail address: dcjia@hit.edu.cn (D. Jia).

0925-8388/$ – see front matter © 2011 Elsevier B.V. All rights reserved.
doi:10.1016/j.jallcom.2011.08.041

Table 1
EDS quantitative analysis for the powder mixture of ZrC, Si, and graphite before and after milling.

Powder mixture	Elemental composition							
	O		Si		Zr		C	
	wt%	mol%	wt%	mol%	wt%	mol%	wt%	mol%
Before milling	0.96	2.10	12.64	15.72	66.93	25.62	19.46	56.57
After milling	1.99	4.56	11.97	15.61	68.95	27.69	17.09	52.14

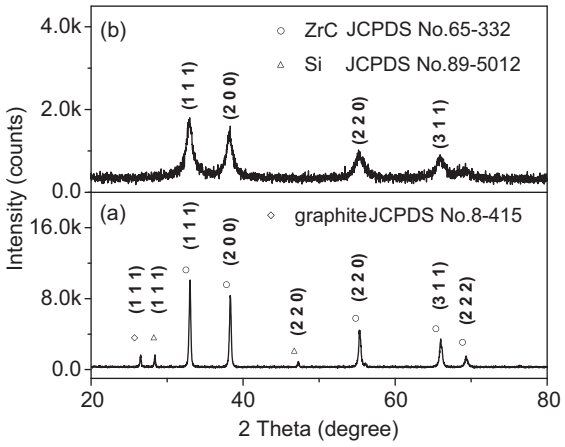

Fig. 1. XRD patterns of the mixed ZrC, Si, and graphite powders before (a) and after (b) milling.

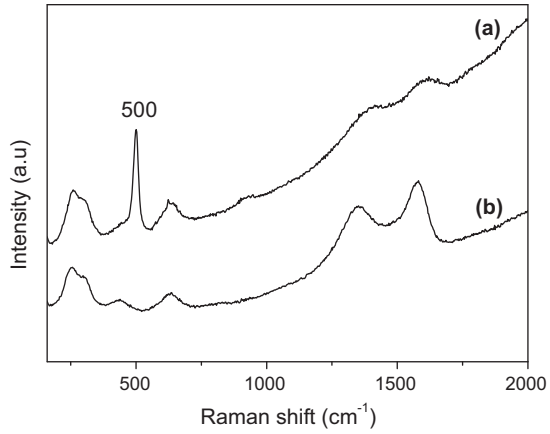

Fig. 2. Raman spectra of the mixed ZrC, Si, and graphite powders before (a) and after (b) milling.

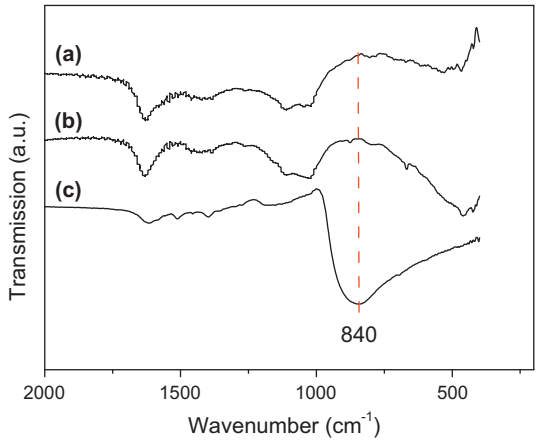

Fig. 3. FTIR spectra of the mixed ZrC, Si, and graphite powders before (a) and after (b) milling, and the mixed Si and graphite powders after milling (c).

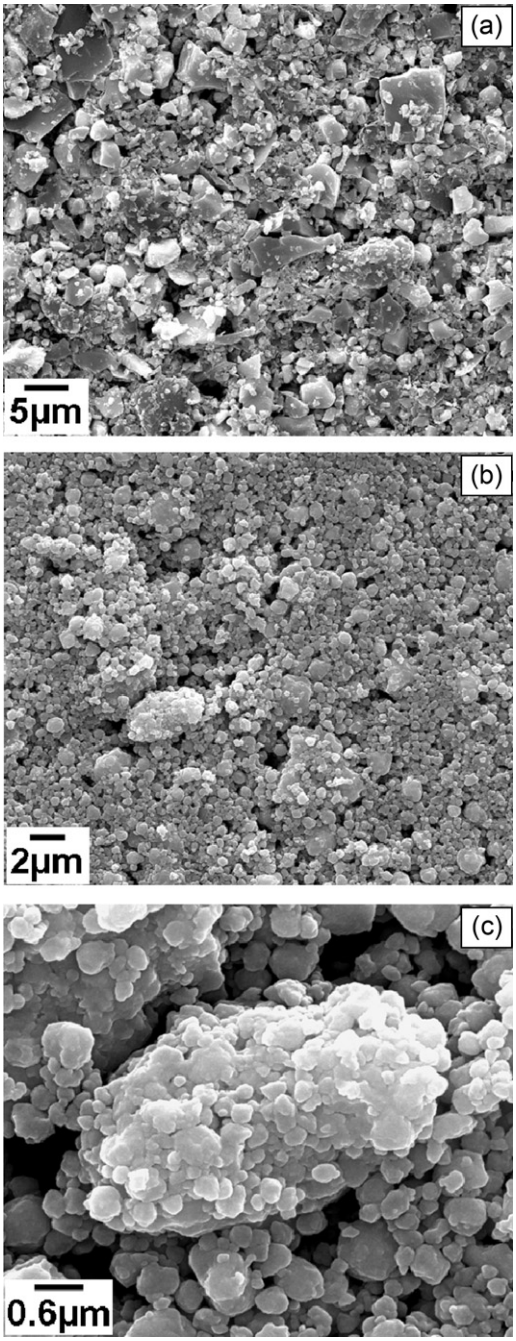

Fig. 4. SEM images of the mixed ZrC, Si, and graphite powders before (a) and after (b) milling. (c) shows the SEM image of agglomerates in milled powders.

3. Results and discussion

Fig. 1 shows the XRD patterns of the powder mixture before and after milling. After high-energy ball milling, peaks of raw ZrC are greatly weakened and broadened, suggesting significant refinement of the ZrC grain size. The diffuse background indicates that there are some amorphous phases in the milled powders. XRD peaks of Si and graphite disappear after high-energy ball milling. This phenomenon can be explained by one or both of the following possibilities. The first is that Si and graphite are transformed into their separate amorphous phases. The second is that reaction of Si with graphite occurs to generate amorphous SiC.

Raman spectrum (Fig. 2) of the milled powders is similar to that of the raw mixed powders except disappearance of Si vibration band at 500 cm^{-1} [17]. Amorphous Si and SiC show weak and broad vibration band in Raman spectra [18–20], so they are difficult to detect by Raman analysis. FTIR analysis is carried out and shown in Fig. 3 to clarify whether reaction between Si and graphite occurs during ball milling. For comparison, a mixture of Si and graphite with molar ratio of 1:1 was high-energy ball milled under above milling conditions. Absorption band at 840 cm^{-1} in Fig. 3(c) corresponds to Si–C stretching [21], indicating that mixed Si and graphite can react to form SiC during milling. However, the mixture of ZrC, Si, and graphite before and after ball milling shows similar FTIR spectra, without obvious SiC absorption band. So, Si and graphite can not achieve a sufficient reaction in the mixture of ZrC, Si, and graphite. This should be attributed to the fact that ZrC decreases the contacts between Si and graphite and consumes collision energy during milling.

Fig. 4 shows the SEM images of the powder mixture before and after milling. The particles of raw powders have an angular shape. The mean particle size is 3.1 μm, measured by laser diffraction technique (Fig. 5). The particles of milled powders have a round shape, and agglomerates are found. The mean particle size is 1.4 μm. EDS quantitative analysis is performed in the whole region of Fig. 4(a) and (b), and the results are shown in Table 1. After ball milling, the O content of powder mixture increases slightly, that is associated with the increase in surface area [22]. The surface area is less than 1 m^2/g for the raw mixed powders, and 6.98 m^2/g for the milled powders. Oxygen is believed to be present as surface oxides produced when new particle surfaces are created during milling. Si content has no obvious change before and after ball milling, indicating the low level of contamination from Si_3N_4 balls/pot. TEM image (Fig. 6(a)) shows many nano-particles embedded in the agglomerates. EDS analysis (Fig. 6(b)) of the agglomerates contains all

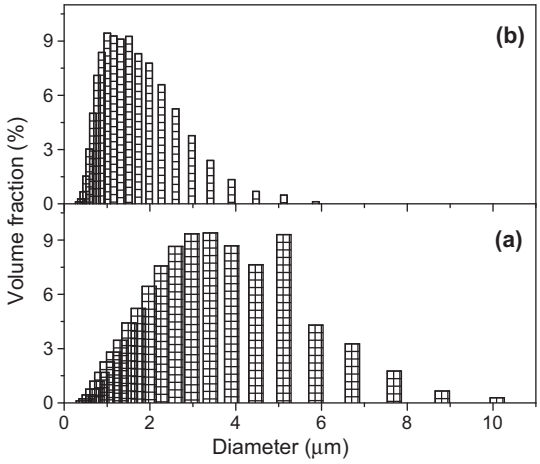

Fig. 5. Particle size distribution of the mixed ZrC, Si, and graphite powders before (a) and after (b) milling.

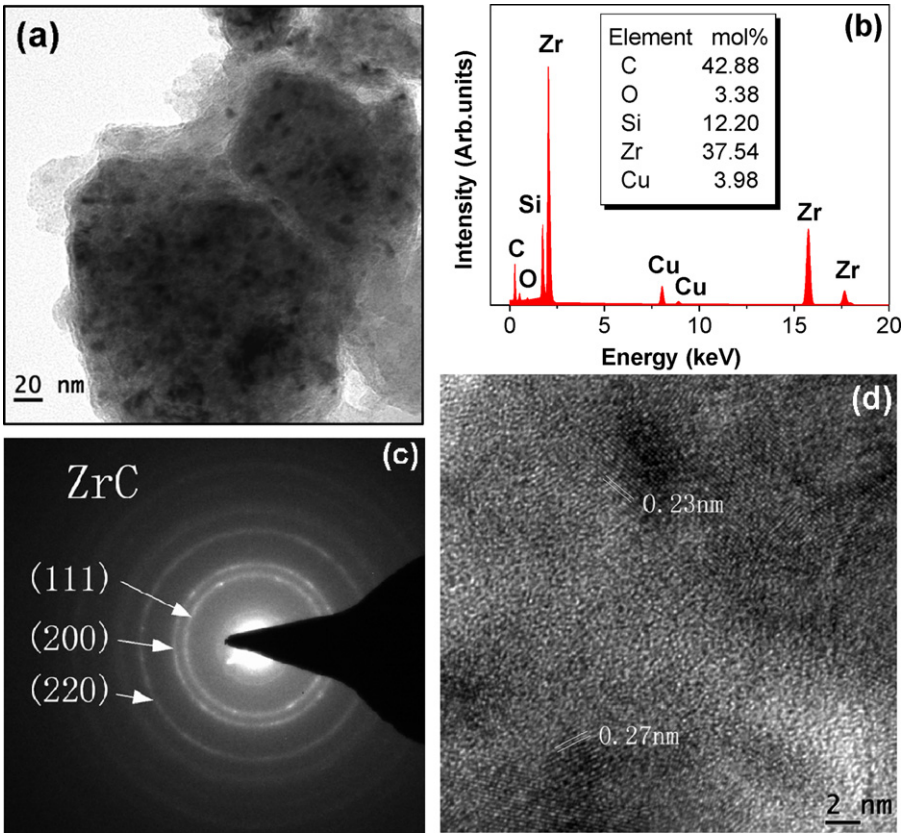

Fig. 6. TEM analysis of agglomerates in the milled powders: (a) TEM image, (b) EDS pattern, (c) SADP, and (d) high-resolution TEM image.

Table 2
Mechanical properties of the obtained ZrC–SiC composite and the reported ZrC-based ceramics in the literature.

Materials	Sintering method	Sintering parameters (°C/min/MPa)	Vickers' hardness (GPa)	Fracture strength (MPa)	Fracture toughness (MPa m$^{1/2}$)	Young's modulus (GPa)
ZrC–30 vol.%SiC	SPS	1800/5/45	18.8 ± 1.2	523.4 ± 19.6	4.0 ± 0.3	390.5 ± 6.9
ZrC [26]	SPS	2100/3/65	17.9 ± 0.6	407 ± 38	–	464 ± 22
ZrC–9 vol.%$MoSi_2$ [26]	SPS	1700/3/100	20.0 ± 0.5	591 ± 48	3.3 ± 0.4	467 ± 22
ZrC–20 vol.%SiC [6]	HP	1900/60/30	19.6	450	3.9	–

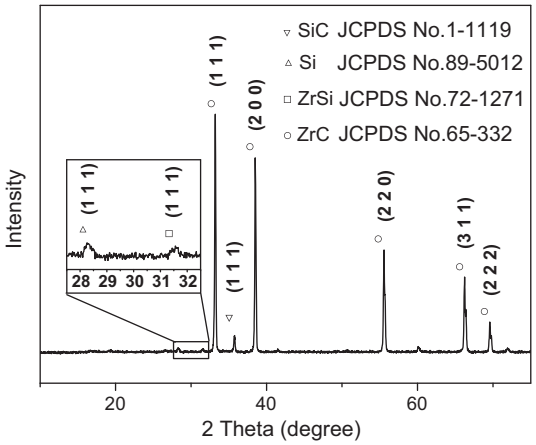

Fig. 7. XRD pattern of the ZrC–SiC composite sintered at 1800 °C.

the elements of raw powders. Because Si element and graphite are present as amorphous phases, selected area diffraction pattern (SADP) of the agglomerates only shows diffraction rings for ZrC (Fig. 6(c)). High-resolution TEM analysis confirms the amorphization of starting powders, but it is difficult to clarify the composition of the observed amorphous phases (Fig. 6(d)).

Fig. 7 shows the XRD pattern of the ZrC–SiC composite sintered at 1800 °C. As expected, the composite mainly consists of ZrC and SiC. Two small peaks are also observed in the XRD pattern, which correspond to Si and ZrSi phases, respectively. Fig. 8(a) shows the SEM image of the polished surface of this composite. Few pores are observed, indicating the good densification of sample. Combining XRD and EDS analysis (Fig. 8(b)), it can be inferred that the light phase is ZrC, and the dark phase is primarily SiC. The fracture surface morphology of the composite sintered at 1800 °C is shown in Fig. 8(c). This composite has a fine microstructure. The mean grain size of ZrC and SiC is less than 1 μm. SiC mainly distributes at the ZrC grain boundaries, but some SiC grains appear within the ZrC grains, forming so-called intragranular structure [23]. The failure mode is a mixture of intergranular and transgranular fracture. TEM analysis (Fig. 9) is conducted to further study the microstructure of the sintered composite. ZrC and SiC grains are confirmed by electron diffraction analysis. But, it is difficult to find the Si and ZrSi phases, though we have done lots of electron diffraction analysis for the Si-containing grains, which are all confirmed as SiC. So, it is believed that the amount of Si and ZrSi in the sintered composite is low, consistent with the weak diffraction peaks in the XRD pattern.

The final density of the composite sintered at 1800 °C is 5.43 g cm^{-3}, that corresponds to a relative density of 96.1%. This value should be smaller than the actual value, because a small amount of low-density phases are present in the composite, such as Si and graphite, which make the theoretical density of composite lower than that used to calculation (5.65 g cm^{-3}). When the sintering temperature is increased to 1900 °C, the relative density does not get a higher value. The densification curve of the ZrC–SiC composite during SPS at 1900 °C is shown in Fig. 10. It can be seen that the shrinkage of the powder compact is completed at 1800 °C which

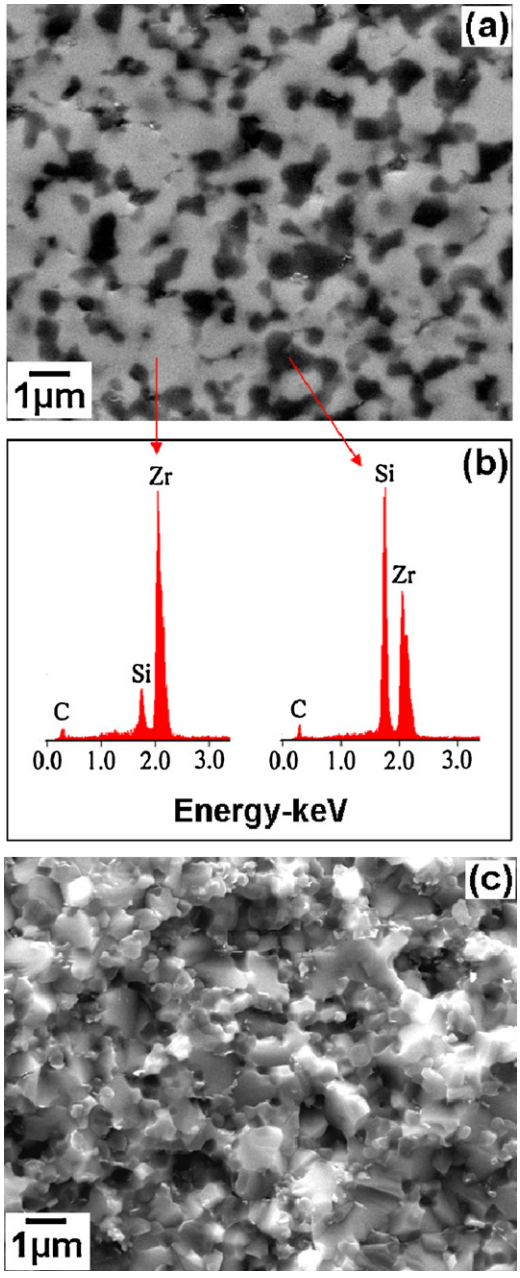

Fig. 8. SEM images of the polished surface (a) and fracture surface (c) of ZrC–SiC composite sintered at 1800 °C. (b) shows EDS patterns of the light and dark phases in (a).

is the optimum sintering temperature. As mentioned above, HEBM and SPS promote densification of materials. Adoption of Si as raw material is also believed to play an important role in this study to lower sintering temperature. Because of the rapid heating, some Si can not react with graphite before they melt. The molten Si could increase the transport rate of materials and thereby enhance the

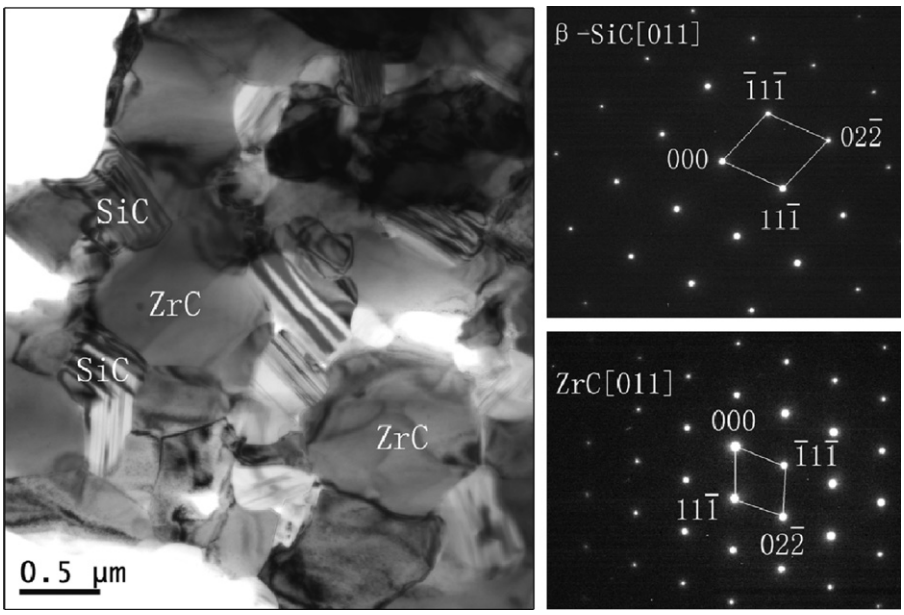

Fig. 9. TEM image of ZrC–SiC composite sintered at 1800 °C with electron diffraction patterns of ZrC and SiC.

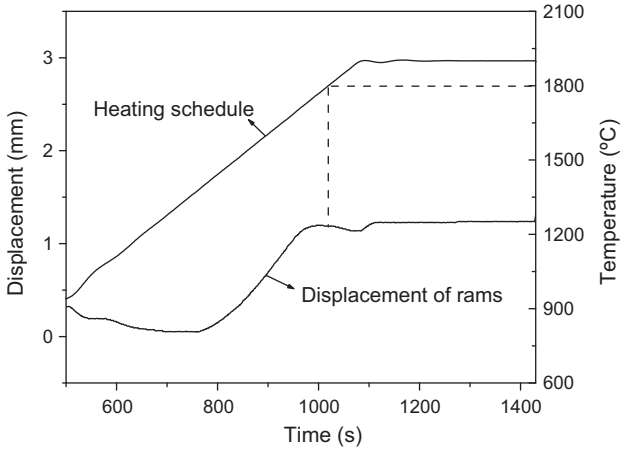

Fig. 10. Densification curve of ZrC–SiC composite during SPS at 1900° C.

sintering rate [24]. ZrC–SiC is sintered to dense fast at relatively low temperature [25].

Room temperature mechanical properties of the obtained ZrC–SiC composite are summarized in Table 2. Previously reported values for ZrC-based composites are also listed in this table. It can be seen that the obtained ZrC–SiC composite has excellent mechanical properties. The excellent mechanical properties are mainly attributable to the fine microstructure and the formation of intragranular structure. The thermal expansion coefficient mismatch between SiC and ZrC matrix can further improve the fracture toughness of composite. The low Young's modulus may be related to the remained Si and graphite in the composite.

4. Conclusion

Zirconium carbide, silicon, and graphite powders were used as raw materials to prepare ZrC–SiC composite. After high-energy ball milling, the particle size of ZrC was significantly refined; most of Si and graphite are transformed into their separate amorphous phases. The milled powders have excellent sinterability. ZrC–30 vol.%SiC was sintered to a relative density of >96.1% at 1800 °C by SPS. The composite exhibited a fine microstructure and excellent mechanical properties. As we know, SiC is an important additive of many ceramics. This work provides a potential method for low-temperature sintering of other SiC-containing composites.

Acknowledgements

This work was supported by the Program for Changjiang Scholars and Innovative Research Team in University.

References

[1] H.O. Pierson, Handbook of Refractory Carbides and Nitrides, William Andrew Publishing/Noyes, Westwood, NJ, 1996, pp. 55-75.
[2] T. Ogawa, K. Ikawa, J. Nucl. Mater. 105 (1982) 331–334.
[3] P. Barnier, C. Brodhag, F. Thevenot, J. Mater. Sci. 21 (1986) 2547–2552.
[4] E. Min-Haga, W.D. Scott, J. Mater. Sci. 23 (1988) 2865–2870.
[5] H.J. Ryu, Y.W. Lee, S.I. Cha, S.H. Hong, J. Nucl. Mater. 352 (2006) 341–348.
[6] B.X. Ma, X.H. Zhang, J.C. Han, W.B. Han, Rare Met. Mater. Eng. 38 (2009) 890–893.
[7] L.Y. Zhao, D.C. Jia, X.M. Duan, Z.H. Yang, Y. Zhou, J. Eur. Ceram. Soc., revised for publication.
[8] B.X. Ma, W.B. Han, Int. J. Refract. Met. Hard Mater. 28 (2010) 187–190.
[9] B.P. Das, M. Panneerselvam, K.J. Rao, J. Solid State Chem. 173 (2003) 196–202.
[10] D. Pizon, R. Lucas, S. Chehaidi, S. Foucaud, A. Maitre, J. Eur. Ceram. Soc., doi:10.1016/j.jeurceramsoc.2010.12.014.
[11] B. Ma, X. Zhang, J. Han, W. Han, J. Aerospace Eng. 223 (2009) 1153–1157.
[12] K.H. Kim, K.B. Shim, Mater. Charact. 50 (2003) 31–37.
[13] I. Khobta, O. Petukhov, O. Vasylkiv, Y. Sakka, A. Ragulya, J. Alloys compd. 509 (2011) 1601–1606.
[14] C.A. Galaïn, A.L. Ortizw, F. Guiberteau, L.L. Shaw, J. Am. Ceram. Soc. 92 (2009) 3114–3117.
[15] A. Moure, J. Tartaj, C. Moure, J. Alloys compd. 509 (2011) 7042–7046.
[16] G.R. Anstis, P. Chantikul, B.R. Lawn, D.B. Marshall, J. Am. Ceram. Soc. 64 (1981) 533–538.
[17] J. Zi, H. Buscher, C. Falter, W. Ludwig, K.M. Zhang, X.D. Xie, Appl. Phys. Lett. 69 (1996) 200–202.
[18] C. Song, Y. Rui, Q. Wang, J. Xua, W. Li, K. Chen, Y. Zuo, Q. Wang, J. Alloys compd. 509 (2011) 3963–3966.
[19] A. Gencer Imer, I. Yildiz, R. Turan, Physica E 42 (2010) 2358–2363.
[20] T. Deschaines, J. Hodkiewicz, P. Henson, Characterization of amorphous and microcrystalline silicon using Raman spectroscopy, Spectroscopy, Thermo Scientific, Madison, WI, USA, 2009 (February 1).
[21] R. Kim, W. Qin, G. Wei, G. Wang, L. Wang, D. Zhang, K. Zheng, N. Liu, J. Cryst. Growth 311 (2009) 4301–4305.
[22] S.C. Zhang, G.E. Hilmas, W.G. Fahrenholtz, J. Am. Ceram. Soc. 89 (2006) 1544–1550.
[23] Q. Liu, W.B. Han, J.C. Han, Scripta Mater. 63 (2010) 581–584.
[24] F. Ye, Z.P. Hou, H.J. Zhang, L.M. Liu, J. Am. Ceram. Soc. 93 (2010) 2956–2959.
[25] M. Gendre, A. Maitre, G. Trolliard, Acta Mater. 58 (2010) 2598–2609.
[26] D. Sciti, S. Guicciardi, M. Nygren, Scripta Mater. 59 (2008) 638–641.